Sensors and Materials, Vol. 35, No. 11 (2023) 3851–3861
MYU Tokyo

S & M 3454

Sensing Behavior of Adsorption/Combustion-type Gas Microsensors to Various Alcoholic Vapors

Takeo Hyodo,[1*] Kazunori Nagae,[1] Taro Ueda,[1]
Takahiko Sasahara,[2] and Yasuhiro Shimizu[1]

[1]Graduate School of Engineering, Nagasaki University,
1-14 Bunkyo-machi, Nagasaki 852-8521, Japan
[2]Gas Equipment R&D Center, Yazaki Energy System Corporation,
23 Minamikajama, Futamata-cho, Tenryu-ku, Hamamatsu-shi, Shizuoka 431-3393, Japan

(Received March 24, 2023; accepted July 25, 2023)

Keywords: adsorption/combustion-type gas microsensor, alcohol, dynamic response, static response, volatile organic compound

Adsorption/combustion-type gas microsensors utilizing γ-Al_2O_3 co-loaded with *m* wt% noble metal and 10 wt% metal oxide [*m*N/10MO/γ-Al_2O_3, N: noble metal (Pd or Pt), MO: metal oxide (CeO_2 or Bi_2O_3)] were fabricated, and their sensor-signal profiles to five types of alcoholic vapor (ethanol, 1-propanol, 1-butanol, 1-pentanol, and 1-hexanol) were investigated and analyzed by differential and integral processing. The sensor-signal profiles largely depended on the types of N and MO as well as the amount of N loaded (*m*). The dynamic response arises from the flash catalytic combustion of the alcohols at 450 °C and their related components (partially oxidized and/or condensed products) adsorbed at 150 °C on the sensing film, and the 10Pt/10CeO_2/γ-Al_2O_3 and 10Pd/10CeO_2/γ-Al_2O_3 sensors showed the largest dynamic responses to 1000 ppm ethanol and 1-hexanol, respectively, among all the sensors tested. These sensors showed sufficiently large dynamic responses even to 10 ppm alcohols. The differential processing of their sensor-signal profiles was valuable in precisely finding slight changes and differences in their sensing behaviors and providing considerable information for data processing.

1. Introduction

Various types of gas sensor (principal sensing material: semiconductor,[1–5] solid electrolyte,[6–10] polymer,[11,12] optical fiber,[13] acoustic resonator,[14] and so on) have been developed to detect volatile organic compounds (VOCs) sensitively and selectively. Among various candidates, our group has specifically focused on improving the VOC-sensing properties of adsorption/combustion-type gas microsensors during the last two decades.[15–23] The adsorption/combustion-type gas microsensors are fabricated by micro-electromechanical system (MEMS) technology. As they can be easily miniaturized with a low power consumption as well as a low heat capacity, they are adequately capable of working under dynamic temperature

*Corresponding author: e-mail: hyodo@nagasaki-u.ac.jp
https://doi.org/10.18494/SAM4403

ISSN 0914-4935
https://myukk.org/

operation to detect a low concentration of VOCs. The large amounts of VOCs are firstly adsorbed on the sensing materials at low temperatures (e.g., room temperature (RT)–150 °C), and subsequently, they burn instantaneously upon pulse heating up to elevated temperatures (e.g., 250–450 °C), which is the origin of the large dynamic response to VOCs. Therefore, the strict compositional and morphological controls of the sensing materials [generally, noble metal (N)-loaded γ-Al_2O_3] were indispensable to effectively oxidize VOCs adsorbed on the surface during the flash heating-up period. We previously demonstrated that the co-loading with Au and Pd on γ-Al_2O_3 by impregnation and the mixing of thermally conductive αAl_2O_3 to the base sensing material, γ-Al_2O_3, were effective in improving the ethanol sensing properties.[18] In addition, the high-dispersed loading with core(Au)/shell(Pd) nanoparticles on γ-Al_2O_3 by utilizing the sonochemical reduction of Au and Pd chlorides with polyethylene glycol monostearate considerably enhanced the sensing properties to ethanol, toluene, and *n*-hexane.[19] Moreover, the co-loading of Pt with one of the various types of metal oxide on γ-Al_2O_3 largely improved the catalytic combustion behavior of VOCs over the oxide surface and thus enhanced the VOC sensing properties.[20–23] On the basis of these previous studies, the effects of the loading of noble metal (Pd or Pt) with metal oxide (Bi_2O_3 or CeO_2) on γ-Al_2O_3 on the sensing properties to five types of alcoholic vapor (ethanol, 1-propanol, 1-butanol, 1-pentanol, and 1-hexanol) have been investigated in this study.

2. Experimental Procedure

2.1 Preparation of sensing materials

Aluminum secondary butoxide [Al(*sec*-$OC_4H_9)_3$, ca. 4.2×10^{-2} mol] and behenic acid ($C_{21}H_{43}COOH$, ca. 1.0×10^{-2} mol) were mixed with 1-propanol (ca. 300 cm^3), and then deionized water (ca. 10 cm^3) was added to the solution. After the solution was stirred at RT for 45 h to hydrolyze Al(*sec*$OC_4H_9)_3$, it was solvothermally treated at 110 °C for 1 h (CEM Corp., MARS5). The white precipitate obtained was washed with ethanol, and then it was fired at 700 °C for 2 h in ambient air, to obtain γ-Al_2O_3 powder. Subsequently, an appropriate amount of bismuth(III) nitrate pentahydrate [$Bi(NO_3)_3{\cdot}5H_2O$] or cerium(III) nitrate hexahydrate [$Ce(NO_3)_3{\cdot}6H_2O$] was mixed with the γ-Al_2O_3 powder in a small amount of deionized water. After they were evaporated to dryness, the precipitates obtained were fired at 700 °C for 1 h in air. The MO-loaded γ-Al_2O_3 powder [MO: metal oxide (Bi_2O_3 or CeO_2)] obtained was denoted as *l*MO/γ-Al_2O_3 [*l*: amount of MO loaded, 10 (wt%) in this study]. Furthermore, Pd or Pt was loaded onto the 10MO/γ-Al_2O_3 powder by impregnation using palladium(II) nitrate dihydrate [$Pd(NO_3)_2{\cdot}2H_2O$] or chloroplatinic(IV) acid hexahydrate, respectively, followed by annealing at 500 °C for 1 h in ambient air. The N-loaded 10MO/γ-Al_2O_3 powder obtained [N: noble metal (Pd or Pt)] was denoted as *m*N/10MO/γ-Al_2O_3 [*m*: amount of N loaded, 1, 5, 10 (wt%) in this study].

2.2 Fabrication of sensors and measurement of sensing properties to various alcoholic vapors

A schematic drawing of the adsorption/combustion-type gas sensor is shown in Fig. 1(a). A microsensor chip was fabricated by MEMS technology. Three thin insulating layers (SiO_2, Si_3N_4, and HfO_2) were deposited on a silicon substrate with a diaphragm structure, and a couple of Pt heaters, which were covered with a thin alumina film, were formed just on the diaphragm structure. The sensing or reference material, i.e., unloaded γ-Al_2O_3 powder, was mixed with an organic vehicle [a mixed solution of di-*n*-butyl phthalate (ca. 36.4 g) and terpineol (ca. 53.6 g) containing polyvinyl butyral resin (ca. 10 g, mean polymerization degree: 700)], followed by ball milling for 30 min. The paste containing an *m*N/10MO/γ-Al_2O_3 or unloaded γ-Al_2O_3 powder was applied over the Pt heaters of the microsensor chip, as a sensing or reference film, respectively, by the drop coating technique employing an air-pulse fluid dispenser (Musashi Eng., Inc., MS-10DX) with a syringe of suitable size, and then the microsensor chips attached with these films were fired at 700 °C for 2 h in ambient air. Hereafter, the sensor is referred to as a sensing material (*m*N/10MO/γ-Al_2O_3).

The sensing properties to alcoholic vapors were measured in an acrylic chamber (inner volume: ca. 50 dm^3), in which five types of target alcoholic vapor (ethanol, 1-propanol, 1-butanol, 1-pentanol, and 1-hexanol; concentration range: 10–1000 ppm) were evaporated with a compact heater. The sensing and reference films with Pt heaters (heat-sensitive elements) of *m*N/10MO/γ-Al_2O_3 sensors were incorporated in a bridge circuit with two fixed resistive elements. All sensors were operated with a mode of pulsed temperature heating [high-temperature operation at 450 °C for 0.4 s after low-temperature (LT) operation at 150 °C for 9.6 s with a cycle of 10 s] by applying a rectangular bridge voltage. Figure 1(b) shows a typical sensor-signal profile of adsorption/combustion-type gas sensors. Alcohols and their related components [partially

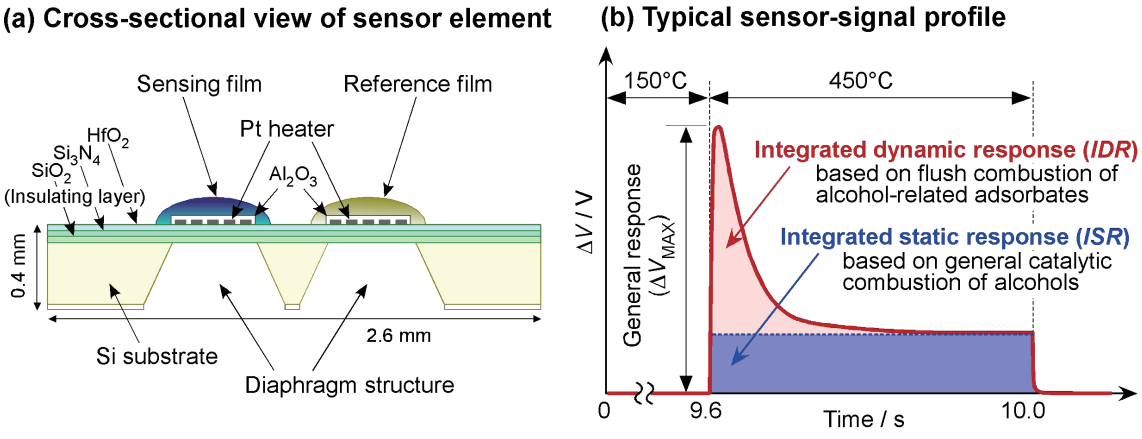

Fig. 1. (Color online) (a) Schematic drawing of adsorption/combustion-type gas sensor and (b) typical sensor-signal profile with definition of three types of response.

oxidized and/or condensed products (intermediates)] in air adsorb on both the sensing and reference materials during the LT period at 150 °C. It is expected that the molecules adsorbed on the sensing material will easily burn upon pulse heating up to 450 °C. Therefore, a sensor-signal profile generally has one dynamic signal, which arises from the flash catalytic combustion of the alcohols and their related components adsorbed on the sensing film, and a subsequent static signal, which arises from the general catalytic combustion of the alcohols during pulse heating at 450 °C. The general response ΔV_{MAX} was defined as the maximum of the difference (ΔV) between output voltages in air containing the alcohols ($V_{alcohol}$) and that in air (V_{air}). Two additional responses calculated by integrating the sensor-signal profiles, i.e., the approximately integrated dynamic response (*IDR*) and approximately integrated static response (*ISR*), were also defined as shown in Fig. 1(b). Moreover, the representative sensor-signal profiles were differentiated with respect to time, especially to elucidate the behavior of the dynamic signal.

3. Results and Discussion

3.1 General response and integrated dynamic and static responses

Figure 2 shows sensor-signal profiles of the 10N/10MO/γ-Al_2O_3 sensors to 1000 ppm ethanol in air. The dynamic responses of the 10Pt/10MO/γ-Al_2O_3 sensors to ethanol were clearly larger than those of the 10Pd/10MO/γ-Al_2O_3 sensors. This indicates that the Pt nanoparticles loaded onto the 10MO/γ-Al_2O_3 surface effectively burned ethanol and its related components [partially oxidized and/or condensed products (intermediates)] adsorbed on the surface during the LT period at 150 °C when the operating temperature instantaneously rose from 150 to 450 °C. In addition, the co-loading of 10 wt% CeO_2 onto γ-Al_2O_3 with N largely enhanced both the dynamic and static responses in comparison with the co-loading of 10 wt% Bi_2O_3 onto γ-Al_2O_3 with N, regardless of the type of N (Pd or Pt). On the other hand, the dynamic and static responses of 10Pt/10MO/γ-Al_2O_3 sensors to ethanol in this study were larger than those of 1Pt/10MO/γ-Al_2O_3 sensors (1Pt/10MO/γ-Al_2O_3: 10MO/γ-Al_2O_3 loaded with 1 wt% Pt by utilizing the sonochemical reduction technique)[20,23] under the same operating conditions, but the difference was not as large as expected from the difference in the amount of Pt between

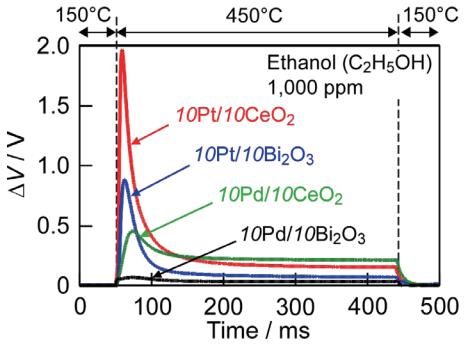

Fig. 2. (Color online) Sensor-signal profiles of 10N/10MO/γ-Al_2O_3 sensors to 1000 ppm ethanol in air.

them. This result probably shows that the dispersibility of Pt nanoparticles loaded by the impregnation technique on the 10MO/γ-Al_2O_3 surface is inferior to that of Pt nanoparticles loaded by the sonochemical reduction technique.

Figure 3 shows the sensor-signal profiles of all 10N/10MO/γ-Al_2O_3 sensors to 1000 ppm large-molecular-weight alcohols (1-propanol, 1-butanol, 1-pentanol, and 1-hexanol) in air. The dependences of ΔV_{MAX}, *IDR*, and *ISR* on the number of carbon atoms of alcohols are also summarized in Fig. 4. Theoretically, the heat of combustion of alcohols increases with the molecular weight (i.e., the number of carbon atoms) of alcohols.[24] ΔV represents an output voltage at a transient time, which is derived from the combustion rate of each alcohol, while the integral of ΔV represents the sum of the combustion heat of the alcohols during a period. Thus, it is expected that the magnitude of responses (especially *ISR*) of adsorption/combustion-type gas sensors will increase with the number of carbon atoms of the alcohols, and thus, it is dependent on the catalytic combustion behavior of the alcohols over the 10N/10MO/γ-Al_2O_3 surface. In addition, ΔV_{MAX} and *IDR* are affected also by the number of carbon atoms of the alcohols and their related components adsorbed on the 10N/10MO/γ-Al_2O_3 surface during the LT period at 150 °C. These factors showed that the observed magnitudes of both the dynamic and static responses of the 10N/10MO/γ-Al_2O_3 sensors were largely dependent on the types of N and MO. As for the 10Pt/10CeO_2/γ-Al_2O_3 sensor, the increase in the number of carbon atoms in alcohols decreased ΔV_{MAX}, delayed the time at which the maximum value of the dynamic profile appeared (e.g., ca. 10 ms and ca. 35 ms from flash heat-up for ethanol and 1-hexanol, respectively), and enhanced the tailing of the dynamic profile. Therefore, the shape of the dynamic response broadened with an increase in the number of carbon atoms of alcohols, and the *IDR* to 1-butanol was the largest of those to all alcohols. Moreover, the *ISR*s of the

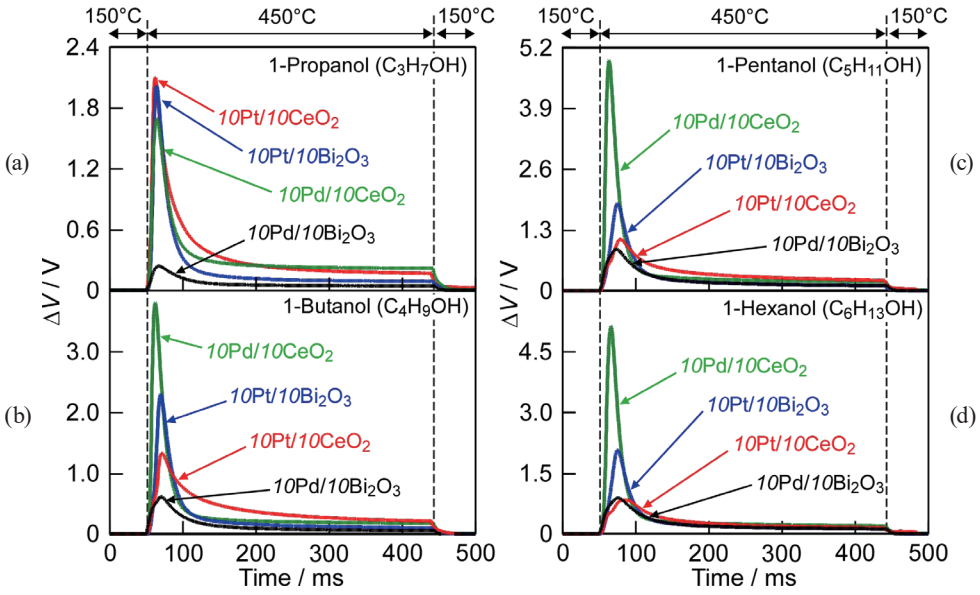

Fig. 3. (Color online) Sensor-signal profiles of 10N/10MO/γ-Al_2O_3 sensors to 1000 ppm (a) 1-propanol, (b) 1-butanol, (c) 1-pentanol, and (d) 1-hexanol in air.

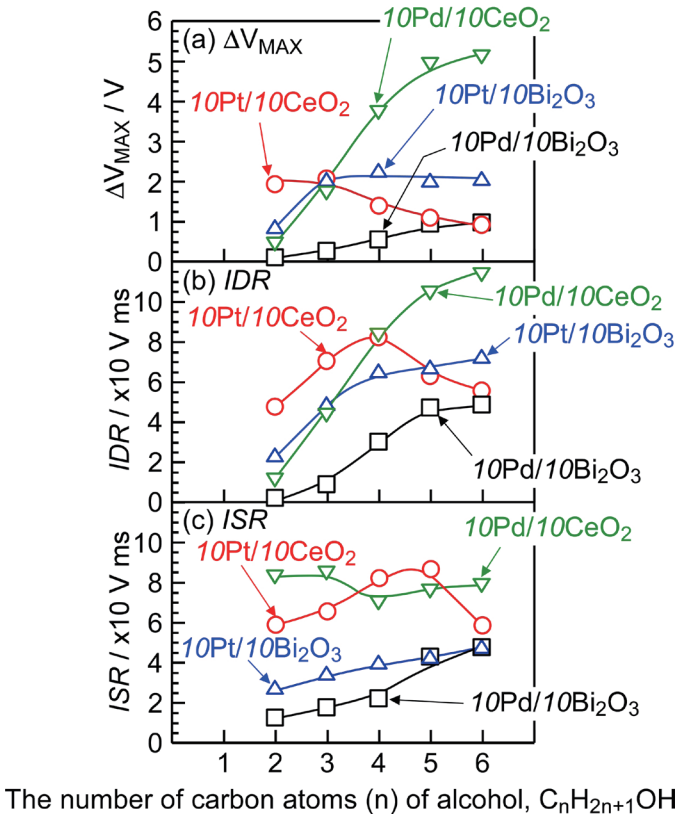

Fig. 4. (Color online) Dependences of (a) ΔV_{MAX}, (b) *IDR*, and (c) *ISR* of 10N/10MO/γ-Al_2O_3 sensors on the number of carbon atoms of alcohols.

10Pt/10CeO_2/γ-Al_2O_3 sensor to 1-butanol and 1-pentanol were also relatively large in comparison with those to ethanol and 1-propanol. These results indicate that the co-loading of Pt and CeO_2 on the γ-Al_2O_3 surface was not effective in burning the large-molecular-weight alcohols and their related components adsorbed on the surface at 150 °C, especially under the dynamic operation.

The ΔV_{MAX} of the 10Pt/10Bi_2O_3/γ-Al_2O_3 sensor tended to be saturated with an increase in the number of carbon atoms of alcohols, and ΔV_{MAX} to large-molecular-weight alcohols was larger than that of the 10Pt/10CeO_2/γ-Al_2O_3 sensor. However, *IDR* gradually increased with the number of carbon atoms of alcohols owing to the delay and widening of the dynamic profiles, which is similar to the behavior of the dynamic responses of the 10Pt/10CeO_2/γ-Al_2O_3 sensor. Thus, the *IDRs* of the 10Pt/10Bi_2O_3/γ-Al_2O_3 sensor to 1-pentanol and 1-hexanol were larger than those of the 10Pt/10CeO_2/γ-Al_2O_3 sensor. *ISR* also gradually increased with the number of carbon atoms of alcohols, and the *ISR* of the 10Pt/10Bi_2O_3/γ-Al_2O_3 sensor to 1-hexanol was comparable to that of the 10Pt/10CeO_2/γ-Al_2O_3 sensor.

The 10Pd/10Bi_2O_3/γ-Al_2O_3 sensor showed the smallest ΔV_{MAX}, *IDR*, and *ISR* among all the sensors. However, all the values gradually increased with the number of carbon atoms of alcohols, and its ΔV_{MAX}, *IDR*, and *ISR* became close to those of the 10Pt/10CeO_2/γ-Al_2O_3 sensor.

On the other hand, the 10Pd/10CeO_2/γ-Al_2O_3 sensor maintained the relatively large *ISR*s to all the alcohols, which hardly depended on the number of carbon atoms, while its ΔV_{MAX} and *IDR* abruptly increased with the number of carbon atoms of alcohols, and the sensor showed the largest ΔV_{MAX} and *IDR* to 1-butanol, 1-pentanol, and 1-hexanol among all 10N/10MO/γ-Al_2O_3 sensors. These results indicate that the co-loading of Pd and CeO_2 on the γ-Al_2O_3 surface was effective in burning the large-molecular-weight alcohols and their related components adsorbed on the surface at 150 °C, especially under the dynamic operation.

Considering these results, the types of N and MO and their combination have a significant impact on the magnitude of responses to these gases, and hereafter, the catalytic combustion behavior of these alcohols over the 10N/10MO/γ-Al_2O_3 surface should be investigated to optimize the composition and microstructure of N and MO loaded on the γ-Al_2O_3 surface.

3.2 Differential sensor-signal profiles

Figure 5 shows the differential sensor-signal (DSS) profiles of 10Pt/10CeO_2/γ-Al_2O_3 and 10Pd/10CeO_2/γ-Al_2O_3 sensors to 1000 ppm ethanol and 1-hexanol in air. As $d\Delta V/dt$ originates from the change in the combustion rate of each alcohol with time, the differential processing of the sensor-signal profiles of these sensors is of considerable significance in precisely understanding the slight changes and differences in their behaviors. The DSS profile of the

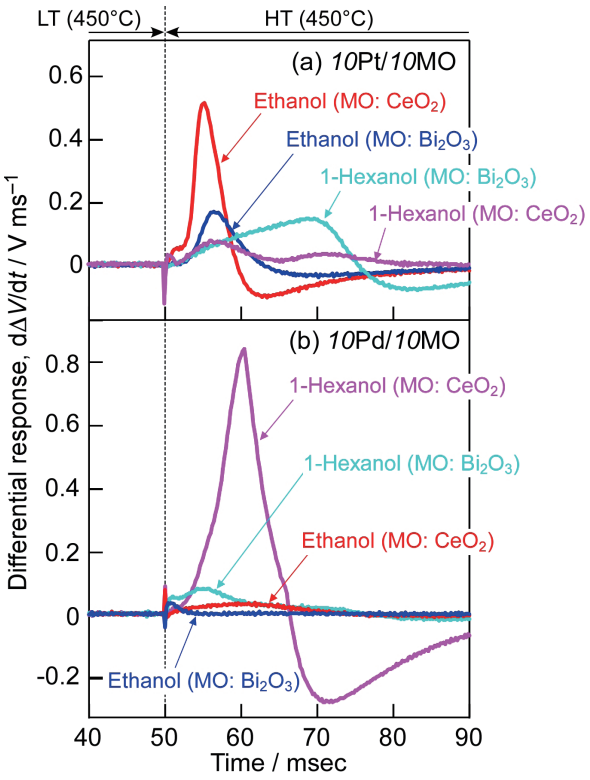

Fig. 5. (Color online) Differential sensor-signal profiles of (a) 10Pt/10MO/γ-Al_2O_3 and (b) 10Pd/10MO/γ-Al_2O_3 sensors to 1000 ppm ethanol and 1 hexanol in air.

10Pt/10CeO_2/γ-Al_2O_3 sensor to ethanol, which showed the largest ΔV_{MAX} to ethanol, consists of a large, narrow, and positive signal and a subsequent broad negative signal, which indicates that the large amount of ethanol and its related components adsorbed abruptly during the LT period as well as efficiently burned on the surface under the dynamic operation. The DSS profile to 1-hexanol of the 10Pt/10CeO_2/γ-Al_2O_3 sensor mainly had two small, broad, and positive signals for 50 ms from flash heat-up, because the small amount of 1-hexanol and its related components adsorbed during the LT period inefficiently burned on the surface. The positive and negative signals in the DSS profile of the 10Pt/10Bi_2O_3/γ-Al_2O_3 sensor to ethanol were smaller than those of the 10Pt/10CeO_2/γ-Al_2O_3 sensor. The 10Pt/10Bi_2O_3/γ-Al_2O_3 sensor had positive and negative signals also in the DDS profile to 1-hexanol. However, the time at which the maximum value of the positive signal appeared markedly delayed and its shape largely broadened, which means that 1-hexanol and its related components adsorbed during the LT period were relatively difficult to burn on the surface in comparison with ethanol and its related components.

The DSS profile of the 10Pd/10Bi_2O_3/γ-Al_2O_3 sensor to 1-hexanol, which was larger than that to ethanol, was comparable to the DDS profile of the 10Pt/10CeO_2/γ-Al_2O_3 sensor to 1-hexanol. The DSS profile of the 10Pd/10CeO_2/γ-Al_2O_3 sensor to ethanol was also too small to be sufficiently analyzed. However, the 10Pd/10CeO_2/γ-Al_2O_3 sensor had a large positive signal and a subsequent large negative signal to 1-hexanol, which was slower than that of the 10Pt/10CeO_2/γ-Al_2O_3 sensor to ethanol. This indicates that a large amount of 1-hexanol and its related components adsorbed on the 10Pd/10CeO_2/γ-Al_2O_3 surface during the LT period, and they were efficiently burned under the dynamic operation.

As mentioned above, the differential processing of the sensor-signal profiles of these sensors to alcohols provides much information on the sensing behavior. Thus, we expect that the differences in these DSS profiles will be useful in identifying the types of alcohol by various data processing techniques with modern Internet-of-Things (so-called IoT) technology.

3.3 Concentration dependences of sensor responses

Figure 6 shows the concentration dependences of the *IDR* and *ISR* of 10Pt/10CeO_2/γ-Al_2O_3, 10Pd/10CeO_2/γ-Al_2O_3, and 10Pd/10Bi_2O_3/γ-Al_2O_3 sensors to all alcohols in air. The *IDR*s of all sensors to all alcohols tend to be saturated with an increase in concentration as shown by auxiliary lines, and such dependences of the *IDR*s on the concentration almost correspond to those of other adsorption/combustion-type gas microsensors in previous papers.[15,16,19,20] This behavior is one of the lines of evidence that the limited numbers of alcohols and their related components could be adsorbed on the surface at 150 °C, and they burned during the flash heating-up period from 150 to 450 °C. In addition, the *IDR*s of the 10Pt/10CeO_2/γ-Al_2O_3 sensor to 10 ppm 1-pentanol and 1-hexanol were larger than those of the 10Pd/10CeO_2/γ-Al_2O_3 sensor, even though the *IDR*s of the 10Pt/10CeO_2/γ-Al_2O_3 sensor to 1000 ppm 1-pentanol and 1-hexanol were smaller than those of the 10Pd/10CeO_2/γ-Al_2O_3 sensor. This might be caused by the differences in the amounts of 1-pentanol, 1-hexanol, and their components adsorbed on the surface under the LT period at 150 °C, which are expected to depend on their oxidation activities

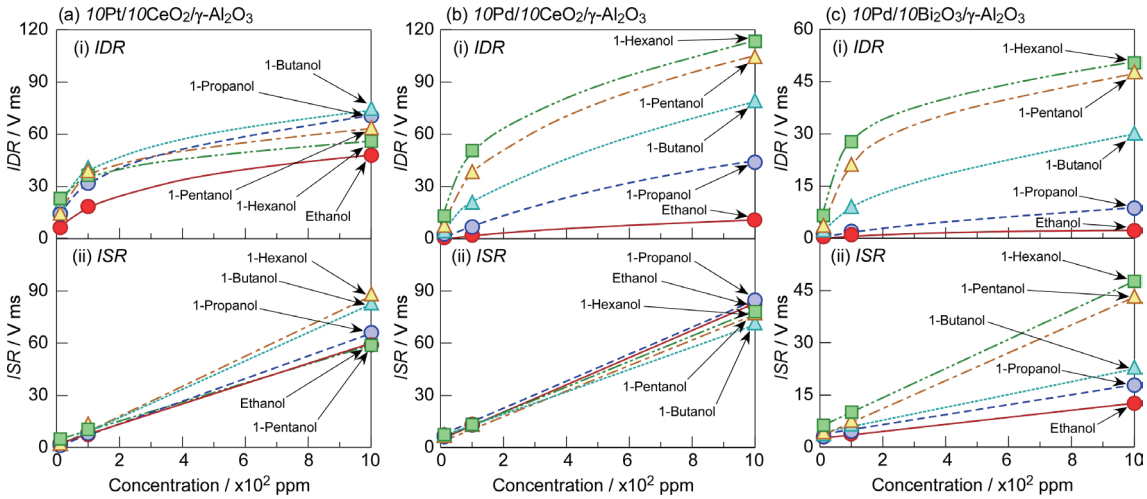

Fig. 6. (Color online) Concentration dependences of *IDR* and *ISR* of (a) 10Pt/10CeO_2/γ-Al_2O_3, (b) 10Pd/10CeO_2/γ-Al_2O_3, and (c) 10Pd/10Bi_2O_3/γ-Al_2O_3 sensors to all alcohols in air.

against the different concentrations of alcohols at 150 °C. In addition, the thickness of the 10N/10CeO_2/γ-Al_2O_3 sensing film of the sensors is also considered to be one of the important factors that affect the magnitude of *IDR*, because the Pt heater (heat-sensitive element) is located beneath the sensing film. On the other hand, the *ISR*s of all sensors to all alcohols increased approximately linearly with the concentration. This is because the alcohols directly burned over the surface during the static operation at 450 °C under pulse heating, which approximately corresponds to that of general catalytic combustion-type gas sensors.[25]

3.4 Effects of amount of N on sensing properties to alcohols

Figure 7 shows the sensor-signal profiles of *m*N/10CeO_2/γ-Al_2O_3 sensors (N: Pd, Pt, *m*: 1, 5, 10) to 10, 100, and 1000 ppm ethanol and 1-hexanol in air. The magnitude of responses (especially ΔV_{MAX} and *IDR*) decreased with a decrease in the amount of N. The tendencies of ΔV_{MAX} and *IDR* were prominent in the high concentration range of both ethanol and 1-hexanol. The behavior indicates that the highly concentrated alcohols are not efficiently oxidized at 450 °C on the surface of *m*N/10CeO_2/γ-Al_2O_3 with the smaller amount of N and that the amounts of alcohols and their related compounds adsorbed at 150 °C are relatively small on the surface. Moreover, the time at which the maximum value of the dynamic response appeared markedly delayed, and the shapes of the sensor-signal profiles to more concentrated 1-hexanol largely changed with a decrease in the amount of Pt, in the case of the sensor-signal profiles of the *m*Pt/10CeO_2/γ-Al_2O_3 sensors. In contrast, the shapes of the sensor-signal profiles of the *m*Pd/10CeO_2/γ-Al_2O_3 sensors to both ethanol and 1-hexanol were not markedly dependent on the concentration. These results also show that the loading of Pd on the 10CeO_2/γ-Al_2O_3 surface is effective in enhancing the sensing properties to 1-hexanol as well as the oxidation activity of 1-hexanol.

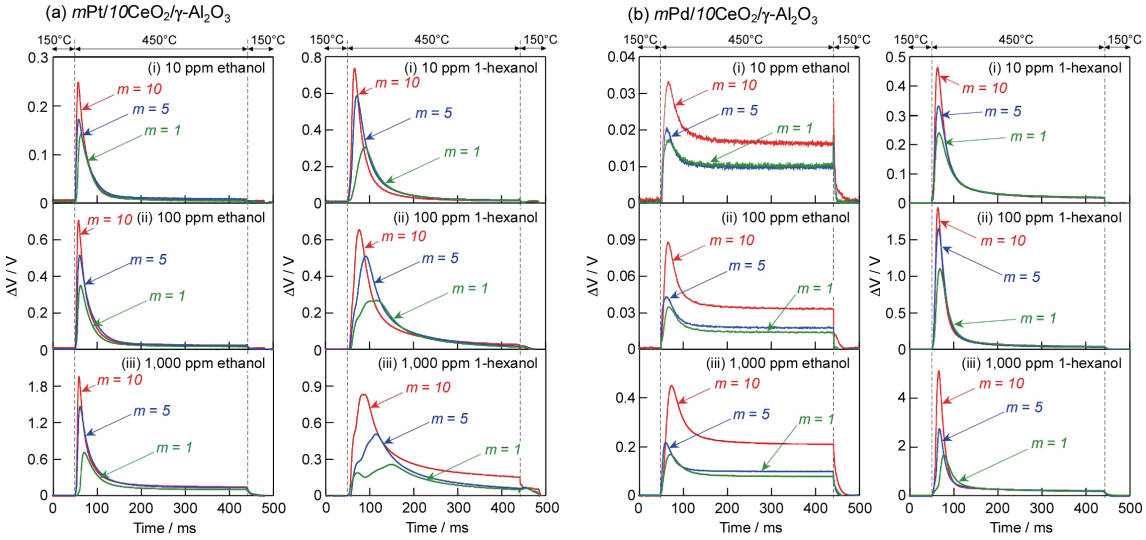

Fig. 7. (Color online) Sensor-signal profiles of mN/10CeO_2/γ-Al_2O_3 sensors [N: (a) Pd, (b) Pt, *m*: 1, 5, 10] to ethanol and 1-hexanol (10, 100, and 1000 ppm) in air.

4. Conclusions

The sensing properties of *m*N/10MO/γ-Al_2O_3 sensors to five types of alcohol (ethanol, 1-propanol, 1-butanol, 1-pentanol, and 1-hexanol) were investigated in this study. The loading of Pt on the 10CeO_2/γ-Al_2O_3 surface largely improved ΔV_{MAX} and *IDR* to ethanol, whereas it was not effective in enhancing ΔV_{MAX} and *IDR* to large-molecular-weight alcohols (1-pentanol and 1-hexanol) as we had expected. Instead, the loading of Pd on the 10CeO_2/γ-Al_2O_3 surface considerably increased ΔV_{MAX} and *IDR* to large-molecular-weight alcohols, especially 1-hexanol, probably owing to the relatively large oxidation activity. These sensors showed sufficiently large responses (especially ΔV_{MAX} and *IDR*) even to 10 ppm alcohols, and the magnitudes and shapes of the sensor-signal profiles were largely dependent on the combination of N and MO as well as the amount of N of the *m*N/10MO/γ-Al_2O_3 sensors. The differential processing of their sensor-signal profiles considerably provided much information on the sensing behavior.

Acknowledgments

This work was supported by JSPS KAKENHI Grant Number JP21H01626.

References

1 A. Schütze, T. Baur, M. Leidinger, W. Reimringer, R. Jung, T. Conrad, and T. Sauerwald: Environments **4** (2017) 20. https://doi.org/10.3390/environments4010020
2 S.-J. Kim, S.-J. Choi, J.-S. Jang, H.-J. Cho, W.-T. Koo, H. L. Tuller, and I.-D. Kim: Adv. Mater. **29** (2017) 1700737. https://doi.org/10.1002/adma.201700737
3 K. Suematsu, Y. Hiroyama, W. Harano, W. Mizukami, K. Watanabe, and K. Shimanoe: ACS Sens. **5** (2020) 3449. https://doi.org/10.1021/acssensors.0c01365

4 S. Torai, T. Ueda, K. Kamada, T. Hyodo, and Y. Shimizu: Chemosensors **11** (2023) 59. https://doi.org/10.3390/chemosensors11010059
5 T. Hyodo, T. Kaino, T. Ueda, K. Izawa, and Y. Shimizu: Sens. Mater. **28** (2016) 1179. https://doi.org/10.18494/SAM.2016.1279
6 T. Kida, T. Minami, S. Kishi, M. Yuasa, K. Shimanoe, N. Yamazoe: Sens. Actuators, B **137** (2009) 147. https://doi.org/10.1016/j.snb.2008.12.014
7 T. Sato, M. Breedon, and N. Miura: J. Electrochem. Soc. **160** (2013) B146. https://doi.org/10.1149/2.007309jes
8 N. Oide, T. Ueda, K. Kamada, T. Hyodo, and Y. Shimizu: Anal. Sci. **36** (2020) 287. https://doi.org/10.2116/analsci.20C003
9 T. Ueda, T. Defferriere, T. Hyodo, Y. Shimizu, and H. L. Tuller: Sens. Actuators, B **317** (2020) 128037. https://doi.org/10.1016/j.snb.2020.128037
10 T. Ueda, N. Oide, K. Kamada, T. Hyodo, and Y. Shimizu: ECS Sensors Plus **1** (2022) 013604. https://doi.org/10.1149/2754-2726/ac63d2
11 M. Kimura, Y. Liu, R. Sakai, S. Sato, T. Hirai, T. Fukawa, and T. Mihara: Sens. Mater. **23** (2011) 359. https://doi.org/10.18494/SAM.2011.743
12 R. Perelló-Roig, J. Verd, S. Bota, B. Soberats, A. Costa, and J. Segura: Lab Chip **21** (2021) 3307. https://doi.org/10.1039/D1LC00484K
13 A. K. Pathak and C. Viphavakit: Sens. Actuators, A **338** (2022) 113455. https://doi.org/10.1016/j.sna.2022.113455
14 G. Zeng, C. Wu, Y. Chang, C. Zhou, B. Chen, M. Zhang, J. Li, X. Duan, Q. Yang, and W. Pang: ACS Sens. **4** (2019) 1524. https://doi.org/10.1021/acssensors.8b01678
15 T. Sasahara, M. Nishimura, H. Ishihara, K. Toyoda, T. Sunayama, S. Uematsu, T. Ozawa, K. Ogino, M. Egashira: Electrochemistry **71** (2003) 457. https://doi.org/10.5796/electrochemistry.71.457
16 T. Sasahara, A. Kido, T. Sunayama, S. Uematsu, M. Egashira, Sens. Actuators, B **99** (2004) 532. https://doi.org/10.1016/j.snb.2004.01.002
17 T. Sasahara, H. Kato, A. Saito, M. Nishimura, M. Egashira, Sens. Actuators, B **126** (2007) 536. https://doi.org/10.1016/j.snb.2007.04.001
18 Y. Yuzuriha, T. Hyodo, T. Sasahara, and Y. Shimizu: Sens. Lett. **9** (2011) 409. https://doi.org/10.1166/sl.2011.1489
19 T. Hyodo, Y. Yuzuriha, O. Nakagoe, T. Sasahara, S. Tanabe, and Y. Shimizu: Sens. Actuators, B **202** (2014) 748. https://doi.org/10.1016/j.snb.2014.06.016
20 T. Hyodo, T. Hashimoto, T. Ueda, O. Nakagoe, K. Kamada, T. Sasahara, S. Tanabe, and Y. Shimizu: Sens. Actuators, B **220** (2015) 1091. https://doi.org/10.1016/j.snb.2015.06.065
21 K. Nagae, T. Ueda, T. Sasahara, O. Nakagoe, S. Tanabe, T. Hyodo, and Y. Shimizu: ECS Trans. **75** (2016) 23. https://doi.org/10.1149/07516.0023ecst
22 T. Hyodo and Y. Shimizu: Anal. Sci. **36** (2020) 401. https://doi.org/10.2116/analsci.19R011
23 T. Hyodo, T. Hiura, K. Nagae, T. Ueda, and Y. Shimizu: J. Asian Ceram. Soc. **9** (2021) 1015. https://doi.org/10.1080/21870764.2021.1933836
24 UKEssays: Effect of Carbon Atoms Number in Alcohol on Combustion (2018). https://www.ukessays.com/essays/chemistry/effect-carbon-atoms-alcohol-combustion-3301.php (accessed March 2023).
25 W. Jang, J.-S. Park, K.-W. Lee, Y. Roh: Micro Nano Syst. Lett. **6** (2018) 7. https://doi.org/10.1186/s40486-018-0069-y